NUCL SCI TECH (2016) 27:137
DOI 10.1007/s41365-016-0131-5

Beam charge integration in external beam PIXE–PIGE analysis utilizing proton backscattering with an extraction window

Ya Xu[1,2] · Mi Xu[1] · Guang-Fu Wang[1,3] · Chen-Long Zheng[1] · Meng-Lin Qiu[1] · Ying-Jie Chu[1]

Received: 22 August 2015 / Revised: 6 November 2015 / Accepted: 22 January 2016 / Published online: 12 October 2016

Abstract In this study, we present a new method for the indirect integration of beam charges in external beam proton-induced X-ray emission and proton-induced γ-ray emission (PIXE–PIGE) analysis. We recorded proton spectra backscattered by a Kapton film extraction window in different sample situations and under different beam currents. We also simulated backscattering spectra using the simulation of backscattering spectra program (SIMNRA). We determined that in a specific geometrical arrangement, different sample situations did not significantly affect factor C_Q (the ratio between integral backscattering proton counts and integral beam charges). We also studied the reproducibility and beam current dependence of factor C_{Q}. The statistic factor of C_{Q} was 28.95 ± 0.6 kilo counts/μC, with a relative standard deviation of 2.0 %. Significantly, in external beam PIXE–PIGE analysis, we were able to calculate beam charge integration from the integral backscattering proton counts in an energy region.

Keywords Beam charge integration · External beam · PIXE–PIGE · Proton backscattering

This work was supported by the Beijing Natural Science Funds (No. 1142006).

✉ Guang-Fu Wang
guangfu_w@bnu.edu.cn

1 College of Nuclear Science and Technology, Beijing Normal University, Beijing 100875, China

2 China Nuclear Power Engineering Co. Ltd., Beijing 100840, China

3 Beijing Radiation Center, Beijing 100875, China

1 Introduction

Quantitative external beam proton-induced X-ray emission and proton-induced γ-ray emission (PIXE–PIGE) analysis has yielded meaningful results in environtology [1, 2], biology [3], art, archaeology [4–7], and many other fields with the aid of integrated beam charges. Several methods have been adopted for measuring beam charge integration in external beam PIXE–PIGE analysis. The Faraday cup is the most traditional method, but it is not applicable to thick samples which beam line cannot penetrate. Past studies have also exploited the Rutherford Back Scattering (RBS) signal of protons (backscattered from helium atoms out of an exit window) to aim and measure beam charge integration. However, with the RBS approach helium pressure must be monitored due to its effect on proton spectrum background levels [8]. In the Laboratorio Beni Culturali (LABEC) laboratory, beam current is inferred from the height of the proton backscattering spectra on the exit window [9]. One method for indirect charge integration employs the light emission from air molecules excited by the proton beam, where the light intensity is relevant to beam energy and gas pressure [10]. Other studies have employed proton-induced X-ray yields on Mylar film (coated with cobalt) [11] and exit windows for charge integration in the determination of the composition of glass [5] and low current measurements [12]. In proton single-event-effects experiments, film scintillators have been applied to detect the proton beam [13]. Finally, in the Japan National Institute of Radiological Sciences (NIRS), the beam current is monitored with a ceramic channel electron multiplier (CEM) to detect secondary electrons from a carbon film [14].

Traditionally, the Faraday cup method is used for beam charge integration in the External Beam PIXE–PIGE

Analysis Facility at the GIC4117 Tandem Accelerator of Beijing Normal University; however, in thick samples situation, the beam charge cannot be integrated directly. Hence, quantitative analysis is difficult to achieve. To solve this problem, we assembled a new proton extraction window. During sample analysis, we installed an Au–Si surface barrier detector in a vacuum to detect the protons backscattered by the Kapton extraction window. At the same time, the actual beam charge (Q_F) was integrated by the Faraday cup. Then, we compared the integration of backscattering proton total counts C_B (corrected for dead time) in a certain energy region to the actual beam charge integration. We then obtained the ratio factor of C_Q (C_B/Q_F, kilo counts/μC, kc/μC). Finally, in sample situations where the beam charge could not be integrated directly, we calculated beam charge integration from the integration of backscattering proton counts and factor C_Q.

2 Experimental setup

The proton beam line used in this study was produced by the GIC4117 Tandem Accelerator of Beijing Normal University (we have already provided details on the pre-existing external beam analysis facility) [1, 15]. In this study, we replaced the extraction window with a 7.5-μm Kapton exit window. We positioned a 20-mm^2 Au–Si surface barrier detector (100 V bias, 0.5 μS shaping time, 302.6 amplifier gain) in vacuum behind the window. This barrier detector covered a fixed solid angle of the exit window. We placed a two-dimensional computer-controlled sample holder 1.2 cm from the exit window. We established a 600 cm^3/min standard-state helium (He) flow between the window and the sample in order to maintain a stable low-Z gas atmosphere. Significantly, this method can lower beam attenuation and improve the detection efficiency of low-energy X-ray [16]. We used a silicon drift detector (80 mm^2 area, 25-μm Dura Be window, FWHM 139 eV at 5.9 keV) and a Si(Li) detector (80 mm^2 area, 25-μm Be window, FWHM 159 eV at 6.4 keV) for the detection of low-energy X-rays and medium–high-energy X-rays, respectively. We detected high-energy γ-rays using an HPGe detector. Figure 1 shows the geometric arrangement of the apparatus.

We vacuumed and installed a −350 V biased Faraday cup behind the sample holder. It is calibrated by X-ray yield of a thin Fe standard reference sample (49 μg cm^2, MicroMatter) [12]. The proton energy was 2.5 MeV during routine analysis. The proton energy diminished by 147 keV when processed through the Kapton film ($C_{22}H_{10}O_5N_2$), and lost 32 keV when processed through the helium flow (Geant4 simulation, $n = 1000$). We adjusted the diameter of the beam spot to 6.8 mm to cover a sufficient sample area, and to satisfy the necessary requirements for the analysis of several types of routine aerosol samples.

3 Results and discussion

3.1 Backscattering proton spectra

In our experiment, we demonstrate that the counting rate of backscattered protons is too high when the beam current exceeds 10 nA. In order to restrict the dead time of the proton detector to less than 3 %, we attached an aluminum collimator (thickness 100 μm, diameter 0.7 mm) to the detector.

First, we placed a 6.3-μm blank Mylar film on the sample holder. We recorded the spectra S under a 9-nA beam current for 1.20 μC Faraday cup charge integration. Figure 2 shows the proton spectrum and the SIMNRA simulation. The colored curves in Fig. 2 are the general and elements-specific simulations. Peak ① indicates the protons backscattered by the helium atoms. The actual height of the helium (He) peak is lower than the simulation height and diminishes more rapidly in lower-energy regions. This can be attributed to the fact that when the distance from the exit window increases, the detector angle to the He volume decreases. The stacking of Peak ② (carbon), Peak ③ (nitrogen), and Peak ④ (oxygen) indicates the protons backscattered by the Kapton film (Kapton film contains carbon). The air impurity in the He flow resulted in shifts of the nitrogen (Peak ⑤) and oxygen (Peak ⑥) peaks in lower-energy regions. Peak ⑤ and Peak ⑥ increased with decreases in the helium flow. The protons backscattered by the Mylar film were carbon (Peak ⑦) and oxygen (Peak ⑧). Because of the shelter provided by the exit device, the solid angle of the Mylar film was very small, which resulted in the peak height being much lower than those in the simulation.

In order to confirm the sample effect on the spectra, we conducted our measurements using a thick lead plate sample. Figure 3a clearly shows that a lead (Pb) peak significantly affects the spectrum.

Moreover, our detection and simulation results demonstrate that the air impurity in the He flow affected the nitrogen (N) and oxygen (O) peaks in low-energy regions. In the initial solid angle arrangement, the samples significantly impacted the Kapton film backscattering proton peak. In other words, spectra were highly sample dependent.

In order to eliminate the effect of samples on the proton backscattering spectra, we adjusted the position of the Au–Si surface barrier proton detector so that it had no solid angle in relation to the sample. We then re-recorded spectra under sample vacancy, Mylar film, and lead (Pb) plate sample situations. Figure 3b clearly shows the effect of this

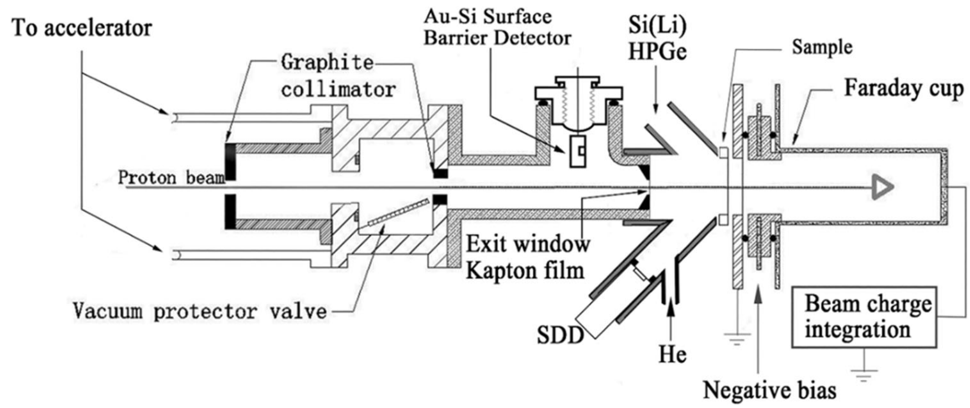

Fig. 1 Sketch of the external beam PIXE–PIGE analysis facility

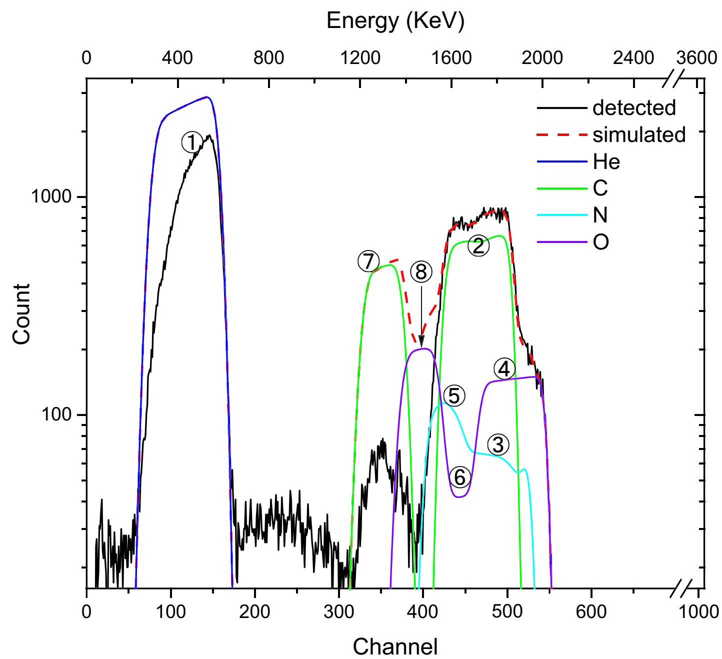

Fig. 2 Mylar film backscattering proton spectrum and simulation in the initial solid angle arrangement

change: No protons backscattered by samples were detected. Additionally, the background level for the Pb plate sample was slightly and continuously heightened. This difference is more noticeable in low-energy sections (most likely because of multiple scattered protons).

Beam-induced thinning of the exit window resulted in a shift of the trailing edges [9]. Furthermore, the PIGE cross section was sensitive to beam energy, which was related to the thickness of the Kapton film. We artificially reduced the density of the Kapton film by 5 % in the simulation, which resulted in shifts in both the He and Kapton peaks. The energy decrease at half of the maximum of the He peak was approximately 21 keV. Thus, in the future, beam-induced thinning of the exit window can be revealed by a shift in the He backscattering proton peak, as well as the FWHM of the exit window peak.

Based on the above results and in order to minimize the effects of air impurity and exit window thinning, we selected the peak area in the channel region (450–555) for proton total count integration.

3.2 Reproducibility under different sample situations

After adjusting the detector position, we recorded proton backscattering spectra under three types of sample situations: sample vacancy, Mylar film, and Teflon film. The beam current was approximately 9 nA, and the

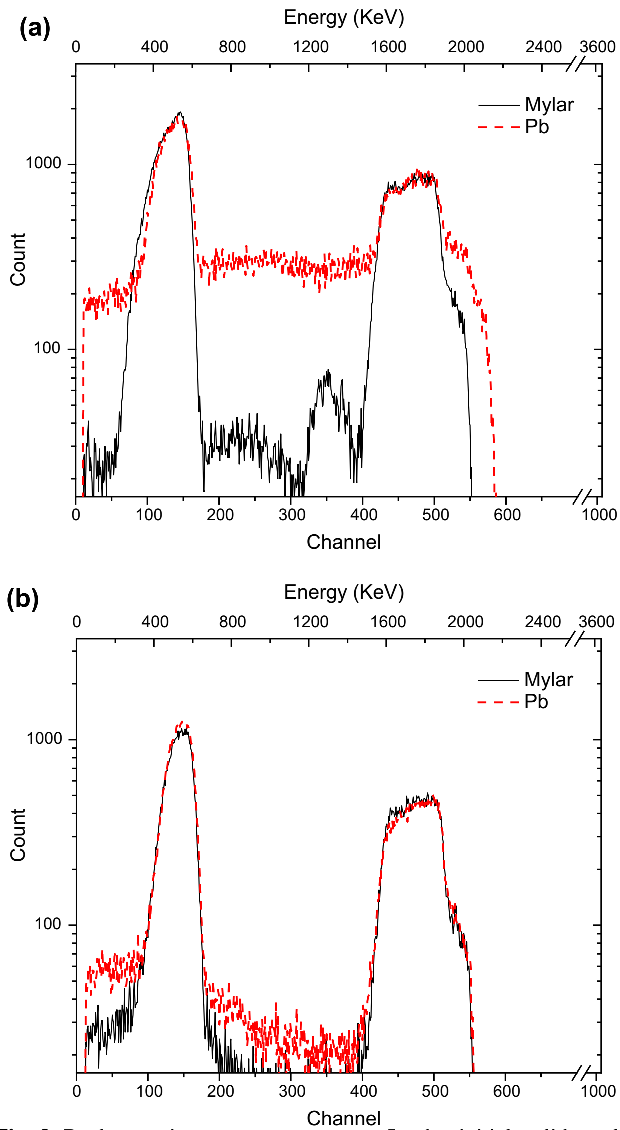

Fig. 3 Backscattering proton spectra: **a** In the initial solid angle arrangement. **b** After the Au–Si surface barrier proton detector was adjusted to have no solid angle to the sample

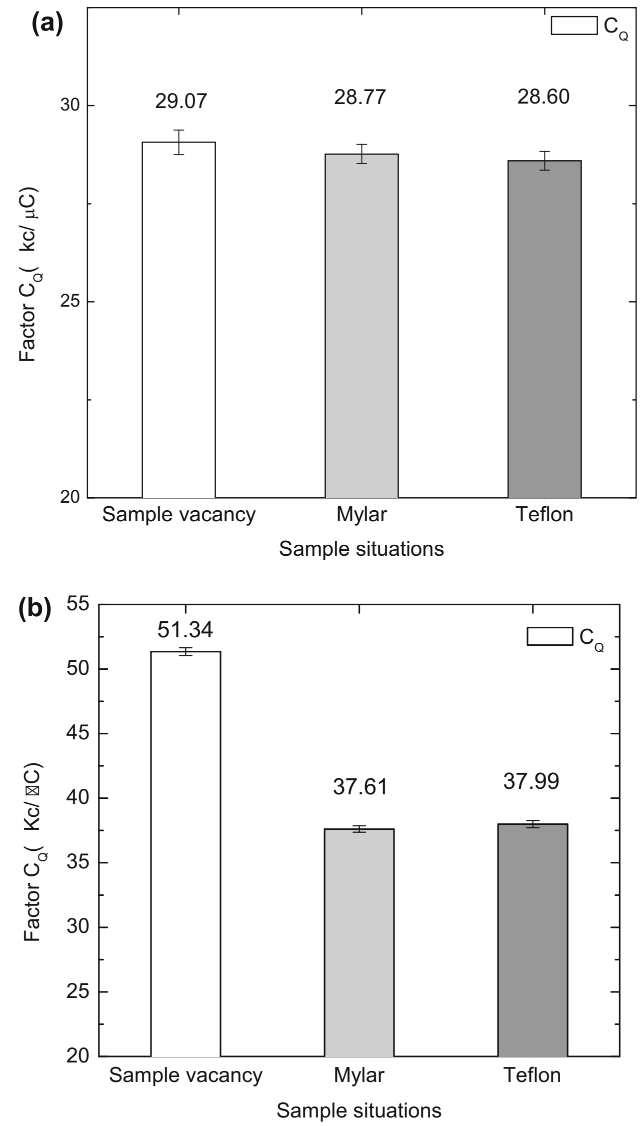

Fig. 4 Specific results of C_Q under the three types of sample situations. **a** Integration region is channel 450–555. **b** Integration region is channel 400–555

Faraday cup beam charge integration was 1.20 μC for every sample. We recorded the spectra five times under each sample scenario.

We integrated the total backscattered protons in channel 450–555. Figure 4a displays high levels of consistency for the specific results. Teflon film spectra were almost identical to Mylar film spectra; however, Teflon film was more fragile. In the sample vacancy situation, the helium atmosphere was diluted by air, and the N and O peaks in the low-energy regions were sharpened. Significantly, different sample situations had no significant effect on factor C_Q when the proton detector had no solid angle in relation to the sample. For comparison to Fig. 4a, the integration of channel 400–555 is shown in Fig. 4b.

3.3 Beam current dependence

Based on the above results, we only studied the beam current dependence of C_Q under the Mylar sample situation. The beam current increased from 2 to 20 nA, which covers the commonly used beam current levels in our laboratory. We recorded five spectra under each beam current, and the beam charge integration was 1.20 μC for every measurement. As shown in Fig. 5, factor C_Q varied from 27.60 to 29.91 kc/μC. The mean value was 28.95 ± 0.6 kc/μC, with a RSD of 2.0 %. In this study, the primary sources for errors are detection errors and charge integration errors.

We observed proton–beam-induced thinning of the Kapton film exit window with the naked eye. Although this proton–beam-induced thinning has not yet resulted in

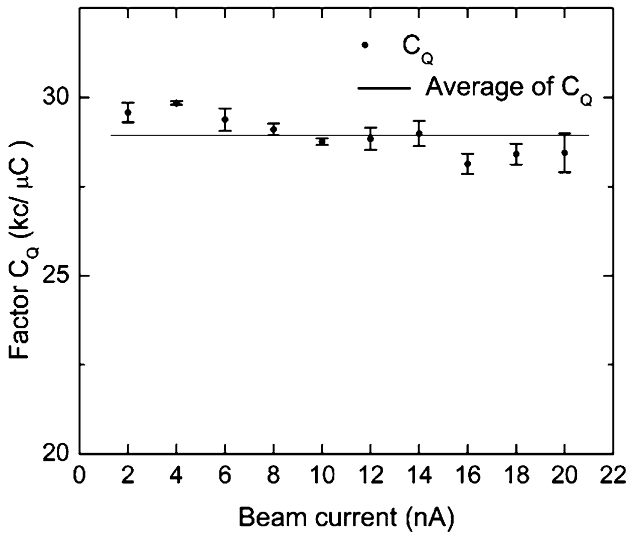

Fig. 5 C_Q (the ratio between integral backscattering proton counts and integral beam charges) as a function of beam current

significant variations in the spectra or factor C_Q, the Kapton film should be replaced periodically to prevent it from bursting and to maintain stable proton energy loss.

Ultimately, our study determined that the value of C_Q can change with different detector solid angles, exit window types, and beam energies; however, the value of C_Q remains constant under a specific geometric arrangement and parameter setting. Additionally, factor C_Q can be revised before analysis if necessary. In the future, we will study the precise measurement of exit window thinning and the beam energy dependence of C_Q.

4 Conclusion

We studied proton backscattering through an extraction window under different sample situations and beam currents in order to determine indirect beam charge integration. By detection and simulation of proton backscattering spectra, we found that the type of sample, Kapton film thickness, He atom density, and air impurity all influence the spectra. By using a precise detector geometric arrangement and selecting the spectra range of interest, C_Q (the ratio between the integral backscattering proton total count and the integral beam charge) tended to be highly consistent in all situations. The influences of the type of sample, air impurity in the helium atmosphere, and proton-induced exit window change were entirely eliminated. Ultimately, the C_Q mean value was 28.95 ± 0.6 kc/μC, with an RSD of 2.0 %. Generally, C_Q is applicable for beam charge integration in external beam PIXE–PIGE analysis. Nondestructive quantitative PIXE–PIGE analysis of thick sample situations is achieved with this system.

References

1. G.F. Wang, X.F. Li, J.H. Chu et al., External beam PIXE/PIGE analysis facility on GIC4117 tandem accelerator. At. Energy Sci. Technol. **48**, 1290–1295 (2014). doi:10.7538/yzk.2014.48.07.1290
2. F. Lucarelli, G. Calzolai, M. Chiari et al., The upgraded external-beam PIXE/PIGE set-up at LABEC for very fast measurements on aerosol samples. Nucl. Instr. Meth. B **318**, 55–59 (2014). doi:10.1016/j.nimb.2013.05.099
3. X.D. Wang, Z.G. Ren, G.H. Tang et al., The trace arsenic element analysis in hairs by external beam PIXE. J. Fudan Univ. (Nat. Sci.) **19**, 351–355 (1980)
4. T. Calligaro, J.P. Poirot, G. Querre, Trace element fingerprinting of jewellery rubies by external beam PIXE. Nucl. Instrum. Methods B **150**, 628–634 (1999). doi:10.1016/S0168-583X(98)01004-0
5. B. Gómez-Tubío, M.Á. Ontalba Salamanca, I. Ortega-Feliu et al., PIXE–PIGE analysis of late roman glass fragments. Nucl. Instrum. Methods B **249**, 616–621 (2006). doi:10.1016/j.nimb.2006.03.068
6. M.A. Rizzutto, M.V. Moro, T.F. Silva et al., External-PIXE analysis for the study of pigments from a painting from the Museum of Contemporary Art. Nucl. Instrum. Methods B **332**, 411–414 (2004). doi:10.1016/j.nimb.2014.02.108
7. L. Quentin, M. Brice, P. Claire et al., Fast mapping of gold jewellery from ancient Egypt with PIXE: searching for hard-solders and PGE inclusions. Talanta **143**, 279–286 (2015). doi:10.1016/j.talanta.2015.04.064
8. B. Hietel, N. Menzel, K. Wittmaack, RBS control of the proton fluence in external PIXE analysis using a He atmosphere. Nucl. Instrum. Methods B **109**, 139–143 (1996). doi:10.1016/0168-583X(95)00895-0
9. G. Calzolai, M. Chiari, I. García et al., The new external beam facility for environmental studies at the Tandetron accelerator of LABEC. Instrum. Methods B **249**, 928–931 (2006). doi:10.1016/j.nimb.2006.03.193
10. J.O. Lill, Charge integration in external-beam PIXE. Nucl. Instrum. Methods B **150**, 114–117 (1999). doi:10.1016/S0168-583X(98)01074-X
11. M.I. Dinator, S.A. Cancino, P.A. Miranda et al., An indirect method to measure the electric charge deposited on insulators during PIXE analysis. Nucl. Instrum. Methods B **263**, 529–531 (2007). doi:10.1016/j.nimb.2007.07.011
12. M. Chiari, A. Migliori, P.A. Mandò, Measurement of low currents in an external beam set-up. Nucl. Instrum. Methods B **188**, 162–165 (2002). doi:10.1016/S0168-583X(01)01067-9
13. L. Zhang, C.H. He, L. Chen et al., In-site measurement of intensity of proton beam using film scintillator. Nucl. Tech. **35**, 21–25 (2012). **(in Chinese)**
14. I. Takahiro, I. Hiroyuki, O. Masakazu et al., Development of a real-time beam current monitoring system for microbeam scanning-PIXE analysis using a ceramic channel electron multiplier. Nucl. Instrum. Methods B **267**, 2032–2035 (2009). doi:10.1016/j.nimb.2009.03.011
15. X.F. Li, G.F. Wang, J.H. Chu et al., Charge integration in external PIXE–PIGE for the analysis of aerosol samples. Nucl. Instrum. Methods B **289**, 1–4 (2012). doi:10.1016/j.nimb.2012.08.009
16. T. Calligaro, J.D. MacArthur, J. Salomon, An improved experimental setup for the simultaneous PIXE analysis of heavy and light elements with a 3 MeV proton external beam. Nucl. Instrum. Methods B **109–110**, 125–128 (1996). doi:10.1016/0168-583X(95)01209-5